[14] a) M. Morra, E. Occhiello, F. Garbassi, *Langmuir* **1989**, *5*, 872. b) J. P. Youngblood, T. J. McCarthy, *Macromolecules* **1999**, *32*, 6800. c) M. Miwa, A. Nakajima, A. Fujishima, K. Hashimoto, T. Watanabe, *Langmuir* **2000**, *16*, 5754. d) I. Woodward, W. C. E. Schofield, V. Roucoules, J. P. S. Badyal, *Langmuir* **2003**, *19*, 3432. e) J. Kim, C.-J. Kim, *Proc.-IEEE Annu. Int. Conf. Micro Electro Mech. Syst.* **2002**, 479.
[15] M. Steinhart, J. H. Wendorff, A. Greiner, R. B. Wehrspohn, K. Nielsch, J. Schilling, J. Choi, U. Gösele, *Science* **2002**, *296*, 1997.
[16] D. Quéré, *Europhys. Lett.* **1997**, *39*, 533.
[17] A. H. Ellison, W. A. Zisman, *J. Phys. Chem.* **1954**, *58*, 503.
[18] D. Bargeman, *J. Colloid Interface Sci.* **1972**, *40*, 344.
[19] O. N. Tretinnikov, *Langmuir* **2000**, *16*, 2751.
[20] R. E. Johnson, R. H. Dettre, *Adv. Chem. Ser.* **1963**, *43*, 136.
[21] D. Quéré, *Langmuir* **1998**, *14*, 2213.
[22] a) W. Chen, A. Y. Fadeev, M. C. Hsieh, D. Öner, J. Youngblood, T. J. McCarthy, *Langmuir* **1999**, *15*, 3395. b) D. Öner, T. J. McCarthy, *Langmuir* **2000**, *16*, 7777.
[23] Z. Yoshimitsu, A. Nakajima, T. Watanabe, K. Hashimoto, *Langmuir* **2002**, *18*, 5818.
[24] C. W. Extrand, *Langmuir* **2004**, *20*, 4017.

Highly Efficient Blue Electroluminescence from Poly(phenylene ethynylene) via Energy Transfer from a Hole-Transport Matrix**

By *Craig A. Breen*, *Jonathan R. Tischler*, *Vladimir Bulović*, and *Timothy M. Swager**

Recent research in polymer-based organic light-emitting diodes (OLEDs) has focused on the use of conjugated polymers, such as poly(phenylene vinylene) (PPV)[1] and poly(*para*-phenylene) (PPP),[2] owing to their high photoluminescence (PL) efficiency in thin films. Poly(phenylene ethynylene) (PPE), another fully conjugated system, exhibits high solution-state quantum yields and typically possesses wider bandgaps than its PPV counterpart, allowing for a bluer emission.[1b] PPEs also exhibit narrower emission spectra than both PPVs and PPPs, which is desirable for saturated color rendering in display applications. To date, however, PPEs have received little attention as potential OLED materials[3] due to reduced emission efficiencies in the solid state, which has been attributed to aggregation phenomena facilitated by the long persistence length[4] and strong π–π stacking of the PPE polymer backbone. Furthermore, the acetylene linkage in PPEs limits the redox properties of these polymers[3c] contributing to a large potential barrier to charge injection, especially for holes. The present study, however, demonstrates that by circumventing the negative aspects of traditional PPEs outlined above, one can realize efficient blue PPE electroluminescence (EL).

We recently reported a new polystyrene-grafted PPE system that prevents polymer aggregation, allowing for a dramatic increase in the solid-state quantum efficiency.[5] Scheme 1 illustrates two dialkoxy PPEs, along with their respective grafted counterparts, we have synthesized for this study; one with a comonomer with *para*-substitution (*P*-PPE and *GP*-PPE) and another with *ortho*-substitution (*O*-PPE and *GO*-PPE), which further blue-shifts the emission.[6] Table 1 contains characterization data for the synthesized polymers. Comparing the solution- and solid-state photophysical data for these polymers demonstrates that the grafting process isolates the PPE backbone causing the grafted PPE to maintain its solution-state emission and quantum yield in the solid state. Furthermore, by eliminating the intrinsic aggregation of the PPE backbone, grafted PPEs are miscible with other materials systems,[5] allowing for increased compatibility as well as an opportunity to exploit energy transfer in

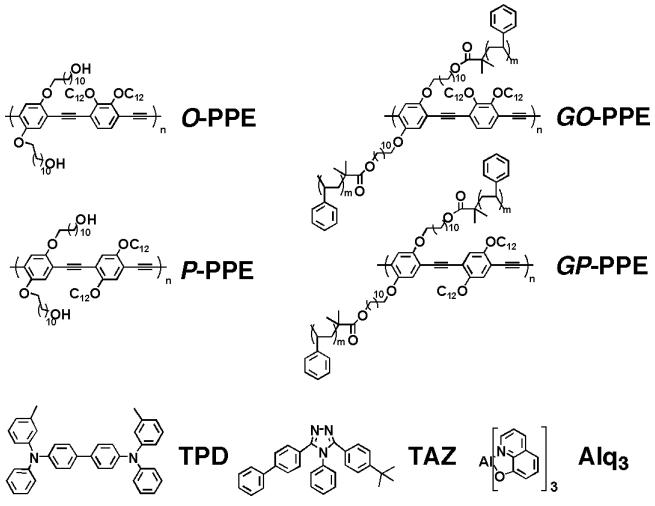

Scheme 1. The structures of *ortho*- (*O*-) and *para*- (*P*-) PPE, and their respective grafted counterparts, *N*,*N*′-diphenyl-*N*,*N*′-bis(3-methylphenyl)-[1,1′-biphenyl]-4,4′-diamine (TPD), 3-(4-biphenyl)-4-phenyl-5-*tert*-butylphenyl-1,2,4-triazole (TAZ), and tris(8-hydroxyquinoline)aluminum) (Alq_3) used in the study.

[*] Prof. T. M. Swager, C. A. Breen
Department of Chemistry
and Institute for Soldier Nanotechnologies
Massachusetts Institute of Technology
Cambridge, MA 02139 (USA)
E-mail: tswager@mit.edu
J. R. Tischler, Prof. V. Bulović
Laboratory of Organic Optics and Electronics
Department of Electrical Engineering and Computer Science
and Institute for Soldier Nanotechnologies
Massachusetts Institute of Technology
Cambridge, MA 02139 (USA)

[**] This work was supported by the U.S. Army through the Institute for Soldier Nanotechnologies, under Contract DAAD-19–02–0002 with the U.S. Army Research Office and MIT MRSEC Program of the National Science Foundation under award number DMR 02–13282.

 DOI: 10.1002/adma.200500185

ADVANCED MATERIALS

Table 1. Polymer characterization. GPC: gel permeation chromatography; M_n: number-average molecular weight; PDI: polydispersity index; λ_{abs}: maximum absorption wavelength; λ_{em}: maximum emission wavelength; Φ: PL quantum yield.

Polymer	GPC analysis		Photophysical characterization					
			Solution state [a]			Solid state		
	M_n [g mol^{-1}]	PDI	λ_{abs} [nm]	λ_{em} [nm]	Φ	λ_{abs} [nm]	λ_{em} [nm]	Φ
O-PPE	85 000	3.50	430	455	0.68	463	472	0.20
GO-PPE	128 000	2.18	430	455	0.57	430	456	0.50
P-PPE	52 000	2.70	450	475	0.70	483	498	0.10
GP-PPE	124 000	1.90	450	475	0.62	450	476	0.60

[a] Measurements carried out with chloroform as the solvent.

the solid state. This paper illustrates the utility of grafted PPEs relative to their ungrafted counterparts by exploring energy transfer from a commonly used hole-transport material, TPD,[7,8] in both PL and EL.

The luminescence of TPD has a significant spectral overlap with the absorption of the PPEs used in this study. Thus, efficient Förster energy transfer from the TPD to the PPEs should be observed provided that the two systems are miscible. In order to investigate energy transfer to the various PPEs, a blend of TPD and PPE (50:50 w/w) was made in chloroform solution (10 mg mL^{-1} total concentration) and deposited onto a glass substrate via spin-casting. The steady-state absorption and PL measurements of these films are plotted in Figure 1. The absorption spectra of the ungrafted PPEs (Figs. 1a,b) reveal characteristic aggregation bands at wavelength $\lambda = 465$ nm and $\lambda = 484$ nm for *O*-PPE and *P*-PPE, respectively, while the grafted PPEs (Figs. 1c,d) maintain their solution-state absorption bands. The PL spectra were obtained by irradiating each film with $\lambda = 360$ nm and $\lambda = 420$ nm light, exciting the TPD and PPE, respectively. The films containing the ungrafted PPEs reveal a significant spectral contribution due to TPD upon excitation at $\lambda = 360$ nm. In addition, the emission intensity of the PPE is not significantly changed when selectively exciting the PPE (when accounting for background TPD emission), suggesting that there is very little energy transfer from TPD to PPE, most likely resulting from spatial segregation of TPD and PPE in the films. Ungrafted PPEs are, therefore, incompatible with the TPD host, as is typical of traditional PPE systems. In the grafted PPE case (Figs. 1c,d), minimal TPD emission is observed when excited at $\lambda = 360$ nm and the significant increase in intensity of PPE emission relative to that under $\lambda = 420$ nm excitation illustrates that this system is thoroughly mixed and undergoes efficient energy transfer. The grafted PPEs are, therefore, compatible with TPD, suggesting that the mixed TPD/grafted-PPE film may display superior spectral purity and operating efficiency in appropriate device architectures.

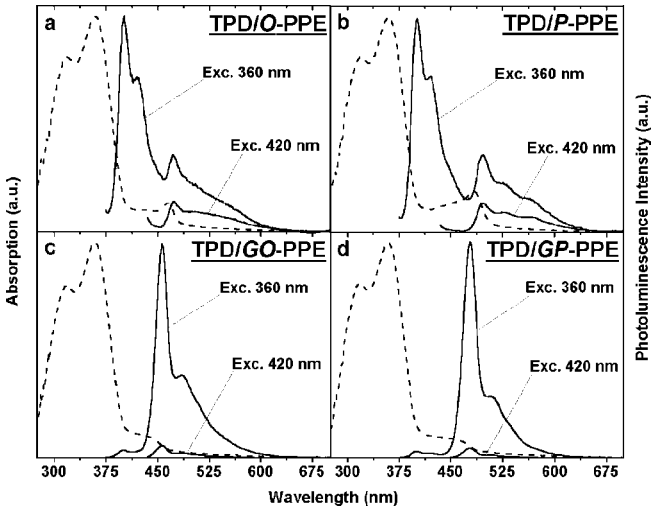

Figure 1. Solid-state absorption and PL spectra of the various TPD/PPE blends. Dashed lines indicate absortption spectra. PL spectra were obtained by irradiating the samples with $\lambda = 360$ nm and $\lambda = 420$ nm excitation wavelengths. a,b) Blends of ungrafted PPE (*O*-PPE and *P*-PPE, respectively). c,d) Blends of grafted PPE (*GO*-PPE and *GP*-PPE, respectively).

The same materials systems were explored in EL devices (device structure is shown in Fig. 2). The hole-transporting TPD/PPE layer is deposited by spin-casting the same blend used for the PL energy-transfer study described above onto indium tin oxide (ITO)-coated glass substrates. This is followed by thermal evaporation of a hole-blocking layer composed of TAZ, an electron-transport layer of Alq_3, and metal electrodes.

The EL spectra of the TPD/PPE devices are shown in Figure 2. For comparison, the inset in Figure 2b shows the emission spectrum of a TPD control device. The control was fabricated with the same device architecture and using a TPD concentration identical to that used to make the TPD/PPE blends (5 mg mL^{-1}). The devices containing ungrafted PPEs exhibit the expected TPD emission component along with PPE emission. In addition, the *O*-PPE device (Fig. 2a) also exhibits a strong spectral component centered at $\lambda = 528$ nm due to aggregate emission. The grafted PPE devices (Figs. 2c,d) exhibit predominantly PPE emission with a minimal TPD component. The EL closely matches the PL spectra, resulting in spectrally pure, narrow blue PPE EL that has not been obtainable with traditional PPE systems to date.[3] The emission for these devices corresponds to Commission Internationale de l'Eclairage (CIE) coordinates of (x= 0.17; y= 0.20) and (x = 0.17; y = 0.35) for *GO*-PPE and *GP*-PPE, respectively. This matches the performance of many current blue display sub-pixels and is close to the National Television System Committee (NTSC) standard blue pixel coordinates of (x = 0.15; y = 0.07). Note that the CIE coordinates of the PL spectra are even bluer (*GO*-PPE: x = 0.16; y = 0.16. *GP*-PPE: x = 0.14; y = 0.28) as the EL devices have not been optimized for the weak microcavity effects that in these structures emphasize green emission.[9]

The current-density–voltage luminance characteristics of the EL devices are plotted in Figure 3. The inset shows the current–voltage characteristics for the four TPD/PPE devices,

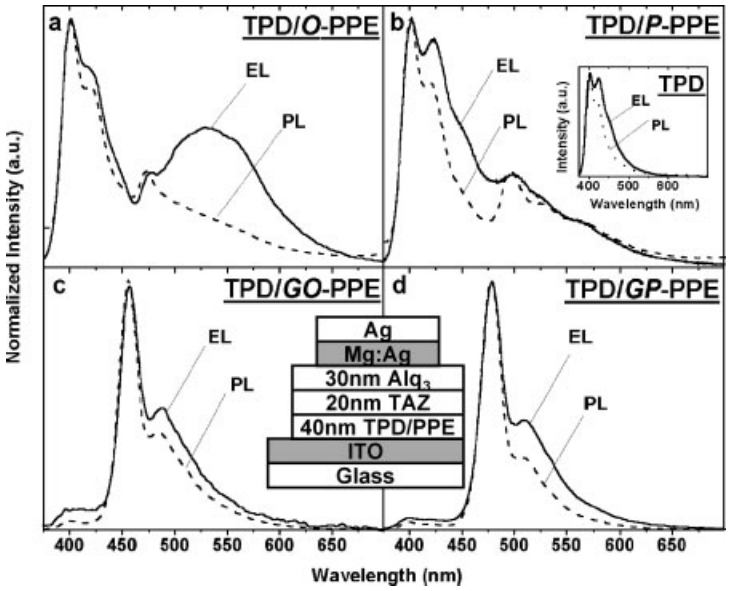

Figure 2. EL spectra (solid line) overlayed with the corresponding PL spectra (dashed line) of the various TPD/PPE LEDs. a,b) Spectra for ungrafted PPE devices (*O*-PPE and *P*-PPE, respectively). Inset to (b): plot of the EL and PL of a TPD control device. c,d) Spectra for devices containing grafted PPE (*GO*-PPE and *GP*-PPE, respectively). Inset: device structure. The TPD/PPE layer is spin-cast onto clean, indium tin oxide (ITO)-coated glass substrates with a thickness of 50 nm for ungrafted PPE blends and 40 nm for grafted PPE blends. This is followed by thermal evaporation of a 20 nm thick film of TAZ, a 30 nm thick film of Alq_3, and a 1 mm diameter, 100 nm thick Mg:Ag (10:1 by mass) cathode, with a 30 nm Ag cap. The spin-casting and device manipulation during fabrication is conducted in a dry-nitrogen environment, with moisture and oxygen content of less than 5 ppm. All EL measurements were carried out in air.

as well as the TPD control device. The ungrafted PPE devices have large leakage currents and high turn-on voltages (~10 V). Furthermore, the external quantum efficiencies for these devices are poor, with peak efficiencies of $\eta = 0.006$ % and $\eta = 0.0007$ % at 100 mA cm^{-2} for the *O*-PPE and *P*-PPE devices, respectively. The higher operational efficiency of the *O*-PPE versus the *P*-PPE may be a result of the higher PL quantum efficiency (see Table 1) of the *O*-PPE. Another factor may be the additional EL of the *O*-PPE aggregate shown in Figure 2. It should also be noted the results presented for ungrafted PPE devices are the best performance out of a low-yield sample. Most devices with ungrafted PPEs on the same substrate would short, have exceedingly high turn-on voltages (> 30 V), or simply not turn on. The low yield is most likely a result of phase separation of the TPD/PPE blend in conjunction with the poor conduction properties of the PPE backbone. An effort to improve upon the fidelity of these devices by reducing the amount of PPE in the TPD blend resulted in strictly TPD luminescence.

The grafted PPE devices have a markedly better behavior. EL devices with the two grafted PPEs have matching current-density–voltage characteristics, with low turn-on voltages, and behave similarly to the TPD control, differing only by a slightly higher operating voltage. This can be attributed to a thicker hole-transport layer and charge trapping owing to poorer conduction properties introduced by the presence of the PPE. Furthermore, in contrast to the ungrafted PPE devices, the grafted PPE devices were entirely reproducible, resulting in high device yields and consistent LED performance.

The external quantum efficiencies for the grafted PPE devices exceed that of the control at low device luminances. The peak efficiencies were $\eta = 1.6$ % and $\eta = 1.1$ % at 0.1 mA cm^{-2} for the *GP*-PPE and *GO*-PPE devices, respectively. These devices maintained an efficiency equal to that of the control at its peak of $\eta = 0.8$ % at 8 mA cm^{-2}. At increasingly higher current densities, the efficiencies of the TPD/PPE devices dropped below that of the control. This behavior can be rationalized in the following manner: at low current densities excitons are formed predominantly on the TPD host molecules and energy transfer allows for highly efficient PPE emission. As the current density is increased, charge is increasingly trapped at the PPEs. Subsequent energy transfer from TPD to charged PPE sites results in a non-radiative Auger process decreasing the external EL efficiency. Thus, the trend continues, since the increase in injected charged species increases the exciton–polaron interaction.[10]

This explanation is supported further when comparing the two grafted PPE devices. At low current densities, the *GP*-PPE device exhibits a higher external quantum efficiency than that of the *GO*-PPE, likely owing to less efficient exciton energy transfer from the TPD to the *GO*-PPE, a result of reduced spectral overlap. However, as the current density is increased the efficiencies of the two devices become equivalent. In other words, at higher current densities the energy transfer from the TPD host plays a less significant role in the device efficiency — due to an increase in direct exciton formation on the PPEs — and thus the two grafted PPE devices exhibit essentially the same behavior.

The device performance of the TPD/PPE systems is in agreement with the PL energy-transfer study and demonstrates the utility of grafted PPE systems over traditional PPEs. While the ungrafted PPE systems displayed poor device operation, the grafted PPE devices exhibited efficient Förster energy transfer resulting in spectrally pure, blue EL with high external quantum efficiencies. Despite the drop in device efficiency with increasing current, the grafted PPE devices are still considerably more efficient at higher luminances than their ungrafted counterparts, as well as other reported PPE systems.[3c]

In summary, we have demonstrated efficient energy transfer from a hole-transport host to grafted PPEs, yielding highly quantum efficient blue electroluminescence. By grafting the PPE backbones and rendering them both quantum efficient in the solid-state as well as miscible with a hole-transport host, we are able to remove the detrimental characteristics of traditional PPE LED systems and realize several orders of magnitude improvement in PPE EL. Furthermore, the grafting process is

ADVANCED MATERIALS

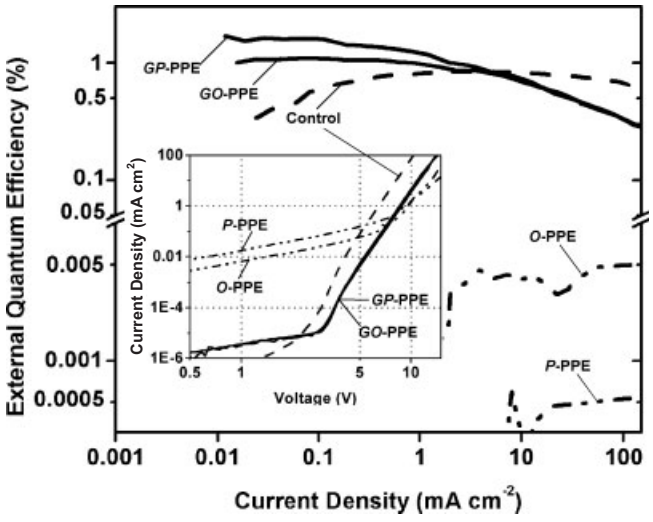

Figure 3. External quantum efficiency versus current density for the TPD/PPE devices and the TPD control device shown in Figure 2. Inset: current–voltage behavior for the various devices. The peak efficiency of the *GP*-PPE device is $\eta = 1.6\,\%$ at 0.1 mA cm^{-2} and 7.5 V, which corresponds to a luminance efficiency of 3.3 cd A^{-1}. The peak efficiency of the *GO*-PPE device is $\eta = 1.1\,\%$ at 0.1 mA cm^{-2} and 7.6 V, which corresponds to a luminance efficiency of 1.7 cd A^{-1}. The ungrafted PPE devices have peak efficiencies of $\eta = 0.006\,\%$ and $\eta = 0.0007\,\%$ at 100 mA cm^{-2} and 16.5 V, which correspond to luminance efficiencies of 0.013 cd A^{-1} and 0.001 Cd A^{-1} for the *O*-PPE and *P*-PPE systems, respectively. The TPD control device has a peak efficiency of $\eta = 0.8\,\%$ at 8 mA cm^{-2} and 7.5 V, giving a luminance efficiency of 0.72 cd A^{-1}.

completely modular. This allows for synthetic flexibility in terms of tuning the PPE backbone structure in order to access other emission wavelengths and materials properties. In light of these results, we believe that PPEs can now be accessed as viable light-emitting materials for OLED applications.

Experimental

General: The general synthesis of the *ortho*- [6] and *para*- [5] monomers, as well as identical procedures used for the preparation of the polymers [5] described here, has been previously reported. The characterization of the polymers used for this study can be found below. ^{1}H NMR spectra for polymers were recorded on a Varian MERCURY (300 MHz) using deuterochloroform as reference or internal deuterium lock. The chemical-shift data for each signal are given in units of δ [ppm] relative to tetramethylsilane (TMS) where δ (TMS) = 0, and referenced to the solvent residual. Infrared spectra were collected with a Perkin Elmer 1000 FT-IR spectrometer in KBr and were recorded in reciprocal centimeters [cm^{-1}, wavenumbers]. UV-vis absorption spectra were measured with a Cary 50 UV/Visible spectrometer. Photoluminescence spectra were measured with a SPEX Fluorolog-τ2 fluorometer (model FL112, 450 W xenon lamp). Solution-state quantum yields were determined relative to Coumarin 314 in ethanol ($\Phi = 0.63$) and solid-state quantum yields were determined relative to $\sim 10^{-2}$ M 9,10-diphenylanthracene in poly(methyl methacrylate) ($\Phi = 0.83$). The molecular weights of polymers were determined using gel-permeation chromatography (GPC) running with tetrahydrofuran as the eluent versus polystyrene standards (Poly-Sciences) using Hewlett–Packard series 1100 HPLC instrument equipped with a Plgel 5 mm mixed-C (300 mm × 7.5 mm) column.

Polymer Characterization O-PPE: IR: ν_{max} 3448, 2923, 2852, 1508, 1466, 1437, 1376, 1262, 1220, 1027, and 803 cm^{-1}; ^{1}H NMR: δ 7.0 (4H, br s), 4.0 (8H, br t), 3.6 (4H, t, *J* 6.7), 1.9 (8H, br multiplet), 1.6–1.5 (16H, br signal) 1.4–1.2 (52H, br signal), 0.9 (6H, t, *J* 6.9); GPC: number-average molecular weight (M_n) 8.50×10^4 g mol^{-1}, weight-average molecular weight (M_w) 2.80×10^5 g mol^{-1}, polydispersity index (PDI, M_w/M_n) 3.50.

O-PPE Atom Transfer Radical Polymerization (ATRP) Macroinitiator: IR: ν_{max} 2923, 2852, 1736, 1509, 1467, 1435, 1389, 1275, 1220, 1163, 1108, 1030, and 805 cm^{-1}; ^{1}H NMR: δ 7.0 (4H, br s), 4.2 (4H, t, *J* 6.6), 4.0 (8H, br t), 1.9 (12H, br s), 1.8 (8H, br t), 1.7 (8H, br signal), 1.5 (8H, br signal), 1.4–1.3 (52H, br signal), 0.9 (6H, t, *J* 6.9).

GO-PPE: IR: ν_{max} 3082, 3060, 3025, 2922, 2851, 1942, 1869, 1780, 1726, 1601, 1493, 1452, 1262, 1027, 803, 756, 697, and 537 cm^{-1}; ^{1}H NMR: δ 7.2–6.9 (aromatic br signal), 6.9–6.3 (aromatic br signal), 4.0 (br t), 3.8 (br t), 2.0–1.7 (br signal), 1.6 (br s), 1.5–1.3 (br signal), 1.27 (br d), 1.0–0.8 (br t); GPC: M_n 1.28×10^5 g mol^{-1}, M_w 2.79×10^5 g mol^{-1}, M_w/M_n 2.18.

P-PPE: ν_{max} 3423, 2923, 2852, 1513, 1468, 1428, 1389, 1340, 1262, 1215, 1026, 858, 802, and 721 cm^{-1}; ^{1}H NMR: δ 7.0 (4H, br s), 4.0 (8H, br t), 3.6 (4H, t, *J* 6.7), 1.9 (8H, br multiplet), 1.6–1.5 (16H, br signal) 1.4–1.2 (52H, br signal), 0.9 (6H, t, *J* 6.9); GPC: M_n 5.20×10^4 g mol^{-1}, M_w 1.40×10^5 g mol^{-1}, M_w/M_n 2.70.

P-PPE ATRP Macroinitiator: IR: ν_{max} 2924, 2853, 1736, 1513, 1466, 1428, 1389, 1275, 1213, 1163, 1108, 1030, 861, 803, and 722 cm^{-1}; ^{1}H NMR: δ 7.0 (4H, br s), 4.2 (4H, t, *J* 6.6), 4.0 (8H, br t), 1.9 (12H, br s), 1.8 (8H, br t), 1.7 (8H, br signal), 1.5 (8H, br signal), 1.4–1.3 (52H, br signal), 0.9 (6H, t, *J* 6.9).

GP-PPE: IR: ν_{max} 3081, 3059, 3026, 2924, 2852, 1943, 1870, 1801, 1730, 1601, 1493, 1453, 1262, 1027, 803, 758, 698, and 539 cm^{-1}; ^{1}H NMR: δ 7.2–6.9 (aromatic br signal), 6.9–6.3 (aromatic br signal), 4.0 (br t), 3.8 (br t), 2.0–1.7 (br signal), 1.6 (br s), 1.5–1.3 (br signal), 1.27 (br signal), 1.0–0.8 (br t); GPC: M_n 1.24×10^5 g mol^{-1}, M_w 2.36×10^5 g mol^{-1}, M_w/M_n 1.90.

Fabrication of Electroluminescent Devices: The devices were built on indium tin oxide (ITO)-coated glass substrates with a sheet resistance of 20 Ω cm^{-2}. The ITO glass was cleaned by ultrasonic agitation in detergent solution, rinsed with deionized (DI) water and acetone, boiled in trichloroethane, rinsed with acetone, boiled in isopropyl alcohol, and blown dry using N_2. Immediately prior to material deposition, substrates were pretreated with UV/ozone for 5 min. The devices were fabricated by spin-casting (velocity: 3000 revolutions min^{-1}; acceleration: 10 000 revolutions min^{-1} s^{-1}) the TPD/PPE layer (50:50 wt./wt.; 10 mg mL^{-1} total concentration), followed by successive vacuum deposition of TAZ (20 nm), Alq_3 (30 nm), Ag:Mg (100 nm; 10:1 by weight), and Ag (30 nm). Prior to deposition, TAZ and Alq_3 were purified by sublimation. A shadow mask with 1 mm^2 openings was used to define the metal electrodes. The EL spectra were recorded on an Acton Research Spectra Pro 300i spectrometer. The luminance–voltage and current-denisty–voltage characteristics were measured on an Agilent-4156C Presision Semiconductor Parameter Analyzer using a Newport 818-UV photodetector. All measurements conducted at room temperature under ambient atmosphere.

Received: January 26, 2005
Final version: April 6, 2005
Published online: June 23, 2005

[1] a) H. Becker, H. Spreitzer, W. Kreuder, E. Kluge, H. Schenk, I. Parker, Y. Cao, *Adv. Mater.* **2000**, *12*, 42. b) A. Kraft, A. C. Grimsdale, A. B. Holmes, *Angew. Chem. Int. Ed.* **1998**, *37*, 402. c) E. G. J. Staring, R. C. J. E. Demandt, D. Braun, G. L. J. Rikken, Y. A. R. R. Kessener, A. H. J. Venhuizen, M. M. F. van Knippenberg, M. Bouwmans, *Synth. Met.* **1995**, *71*, 2179. d) C. Zhang, D. Braun, A. J. Heeger, *J. Appl. Phys.* **1993**, *73*, 5177. e) N. C. Greenham, S. C. Moratti, D. D. C. Bradley, R. H. Friend, A. B. Holmes, *Nature* **1993**, *365*, 628. f) J. H. Burroughes, D. D. C. Bradley, A. R. Brown, R. N. Marks, K. Mackay, R. H. Friend, P. L. Burns, A. B. Holmes, *Nature* **1990**, *347*, 539.

[2] a) Y. Yang, Q. Pei, A. J. Heeger, *J. Appl. Phys.* **1996**, *79*, 934. b) J. Stampfl, S. Tasch, G. Leising, U. Schert, *Synth. Met.* **1995**, *71*, 2125. c) W-X. Jing, A. Kraft, S. C. Moratti, J. Gruner, F. Cacialli, P. J. Hamer, A. B. Holmes, R. H. Friend, *Synth. Met.* **1994**, *67*, 161. d) G. Grem, G. Leising, *Synth. Met.* **1993**, *57*, 4105.
[3] a) E. Arias, T. Maillou, I. Moggio, D. Guillon, J. Le Moigne, B. Geffroy, *Synth. Met.* **2002**, *127*, 229. b) C. Schmitz, P. Posch, M. Thelakkat, H.-W. Schmidt, A. Montali, K. Feldman, P. Smith, C. Weder, *Adv. Funct. Mater.* **2001**, *11*, 41. c) N. G. Pschirer, T. Miteva, U. Evans, R. S. Roberts, A. R. Marshall, D. Neher, M. L. Myrick, U. H. F. Bunz, *Chem. Mater.* **2001**, *13*, 2691. d) X. Zhan, Y. Liu, G. Yu, X. Wu, D. Zhu, R. Sun, D. Wang, A. J. Epstein, *J. Mater. Chem.* **2001**, *11*, 1606. e) S. H. Lee, T. Nakamura, T. Tsutsui, *Org. Lett.* **2001**, *3*, 2005. f) A. Montali, P. Smith, C. Weder, *Synth. Met.* **1998**, *97*, 123. g) M. Hirohata, K. Tada, T. Kawai, M. Onoda, K. Yoshino, *Synth. Met.* **1997**, *85*, 1273. h) S. Tasch, E. J. W. List, C. Hochfilzer, G. Leising, P. Schlichting, U. Rohr, Y. Geerts, U. Scherf, K. Mullen, *Phys. Rev. B.* **1997**, *56*, 4479. i) S. A. Jeglinski, O. Amir, X. Wei, Z. V. Vardeny, J. Shinar, T. Cerkvenik, W. Chen, T. J. Barton, *Appl. Phys. Lett.* **1995**, *67*, 3960. j) K. Yoshino, K. Tada, M. Onoda, *Jpn. J. Appl. Phys., Part 2* **1994**, *33*, 1785.
[4] P. M. Cotts, T. M. Swager, Q. Zhou, *Macromolecules* **1996**, *29*, 7323.
[5] C. A. Breen, T. Deng, T. Breiner, E. L. Thomas, T. M. Swager, *J. Am. Chem. Soc.* **2003**, *125*, 9942.
[6] Z. G. Zhu, T. M. Swager, *Org. Lett.* **2001**, *3*, 3471.
[7] H. Mattoussi, H. Murata, C. D. Merritt, Y. Iizumi, J. Kido, Z. H. Kafafi, *J. Appl. Phys.* **1999**, *86*, 2642.
[8] S. Coe, W.-K. Woo, M. Bawendi, V. Bulovic, *Nature* **2002**, *420*, 800.
[9] V. Bulovic, V. B. Khalfin, G. Gu, P. E. Burrows, D. Z. Garbuzov, S. R. Forrest, *Phys. Rev. B* **1998**, *58*, 3730.
[10] a) S. Tasch, G. Kranzelbinder, G. Leising, U. Scherf, *Phys. Rev. B* **1997**, *55*, 5097. b) M. Deussen, M. Scheidler, H. Bassler, *Synth. Met.* **1995**, *73*, 123.

Single Crystals of ZSM-5/Silicalite Composites**

By *Manabu Miyamoto*, *Takashi Kamei*, *Norikazu Nishiyama*,* *Yasuyuki Egashira*, and *Korekazu Ueyama*

The processes of the formation of dialkylbenzenes from monoalkylbenzene, such as disproportionation and alkylation, are among the most important in the chemical industry. These processes were carried out using solid acid catalysts in earlier times. The activity of these catalysts, such as silica–alumina, was low. Since the late 1960s, ZSM-5 catalysts have been extensively studied because of their much higher selectivity for para-isomers, which are the most valuable compounds for commercial use. However, para-selectivity significantly decreases because of the acid sites on the external surface and the size of the pore openings. Hence, surface modification and pore size control have been proposed in order to enhance the selectivity.[1–9]

On the other hand, zeolites have been studied for membrane separation techniques,[10–13] as well as for catalysis, for a long time. In the last decades, combined chemical reactors with zeolite membranes have been of great interest and a lot of applications have been reported.[14–21] Compared with conventional chemical reactors, membrane reactors have great advantages, such as higher selectivity and/or yield of products, simplification of processes, and inhibition of catalyst poisoning. However, the main issue of membrane reactors is the lower permeation rate than the reaction rate. Due to the low permeation flux, a significantly large membrane area and thin zeolite membrane are required. However, the synthesis of large zeolite membranes without any defects, like pinholes or cracks, and a method of controlling the membrane thickness have not yet been established.

Recently, we have proposed a particle level membrane reactor. A catalyst particle has been coated with a permselective membrane.[22,23] The platinum-loaded TiO_2 particles (particle size = 0.6 mm) coated with a silicalite-1 membrane showed high product selectivity in the hydrogenation of hex-1-ene (1-Hex) and 3,3-dimethylbut-1-ene (3,3-DMB) mixtures. The 1-Hex/3,3-DMB selectivity was 20 because of selective permeation of 1-Hex through the silicalite-1 membrane.[23] Silica–alumina catalyst particles (particle size = 1 mm) were coated with silicalite-1 membranes (silicalite/silica–alumina) and used for the disproportionation of toluene to produce xylene isomers. The silicalite-1 coatings on catalyst particles enhanced the para-selectivity[22] because of selective removal of *p*-xylene through the silicalite-1 membrane. Toluene conversion, however, significantly decreased from 1.5 to 0.08 % with the coating because the thickness of the silicalite-1 membrane was large (40 μm), which limited the diffusion of the products. In addition, the catalytic activity of silica–alumina was not very high.

To solve these problems, in this study we have developed a novel composite catalyst consisting of a zeolite crystal with an inactive thin layer. A silicalite-1 layer was grown on proton-exchanged ZSM-5 crystals (silicalite/H-ZSM-5). The conventional zeolite films on porous supports as well as on the particles[22,23] mentioned above have consisted of an oriented or randomly oriented polycrystalline material. Their film thickness is from several micrometers to several tens of micrometers. On the other hand, in this study a thin layer of zeolite is grown on a small crystal of zeolite, whose crystal size is a few micrometers. The framework structure of the thin layer is the same as that of the substrate. This novel composite is expected to have a very thin layer without a crystal boundary.

Figure 1 shows field-enhanced scanning electron microscopy (FE-SEM) images of uncoated H-ZSM-5 and silicalite/H-ZSM-5 after hydrothermal synthesis for 24 h. The uncoated

[*] Dr. N. Nishiyama, M. Miyamoto, T. Kamei, Dr. Y. Egashira, Prof. K. Ueyama
Division of Chemical Engineering
Graduate School of Engineering Science
Osaka University
1-3 Machikaneyama, Toyonaka, Osaka 560-8531 (Japan)
E-mail: nisiyama@cheng.es.osaka-u.ac.jp

[**] The authors thank M. Kawashima and the GHAS laboratory at Osaka University for the FE-SEM measurements. M. Miyamoto expresses his special thanks for the center of excellence (21COE) program 'Creation of Integrated EcoChemistry of Osaka University'.

 DOI: 10.1002/adma.200500522